EXPERIMENTAL INVESTIGATION OF IONIZATION SENSORS UNDER SHOCK TUBE STAGNATION CONDITIONS

Rafael Augusto Cintra, rafaelcintra94@outlook.com
Universidade Federal de Itajubá, Av. BPS, nº 1303, Bairro Pinheirinho, CEP. 37. 500-903, Itajubá, MG, Brasil

Tiago Cavalcanti Rolim, tiagocrolim@outlook.com
Bruno Coelho Lima, brunocoelho@ieav.cta.br
Instituto de Estudos Avançados, Trevo Coronel Aviador José Alberto Albano do Amarante, nº 1, Putim, CEP. 12.228-001, São José dos Campos, SP, Brasil

Abstract. *Recently, there is a growing interest in studies concerning ionization sensors for aerospace applications, power generation and fundamental research. In aerospace research, they have been used for studies on shock and detonation waves. Two key features of these sensors are their short time response, of the order of microseconds, and the fact that they are activated when exposed to high temperature air. In this sense, this paper describes the development of an ionization sensor to be used in shock tube facilities. The sensor consists of two thorium-tungsten electrodes insulated by a ceramic, with a stainless steel adapter for proper mounting, and two copper seal rings. An electrical circuit was also built with two main purposes: to provide the electrodes with a sufficient large voltage difference in order to ease ionization of the air and to assure a short time response of the sensor. The tests were done in a shock tube with the objective to observe the response of the sensor under stagnation conditions. For that, we chose initial driven pressures of 1.0, 1.2 and 1.5 kgf/cm², with a constant driver pressure equal to 70 kgf/cm². We analyzed the response of the sensor as a function of the initial driven pressure, stagnation temperature and density. For the studied conditions, the results showed that the mean amplitude of the ionization sensor signal varied from 8.29 to 19.70 mV.*

Keywords*: Ionization sensors; Shock tubes; Shockwaves.*

1. NOMENCLATURE

a	Speed of sound
h	Specific enthalpy
M_s	Mach number of incident shockwave
p	Pressure
u	Shockwave speed
u_s	Speed of incident shockwave
u_r	Speed of reflected shockwave
T	Temperature

Greek symbols

Δt	Time interval between pressure sensors signals
Δx	Distance between pressure sensors
ρ	Air density
τ_{charge}	Charge time of the sensor
$\tau_{discharge}$	Discharge time of the sensor

Subscripts

1	Initial driven conditions
2	Conditions after the incident shockwave
5	Conditions after the reflected shockwave

2. INTRODUCTION

Recently, there is a growing interest in the study of ionization sensors for aerospace applications, energy generation and fundamental research. In aerospace research, the ionization sensors are generally used in studies on shock and detonation waves (Gupta, 2013; Panicker, 2008).

In studies of shockwaves the interest lies on the possibility of using these sensors on shock tube improvement since they can detect high temperature air with an appropriate response time. Shock tubes are used for the simulation of the flight conditions of high speed flight, for example, atmospheric vehicle reentry. In fact, this kind of facility can create high stagnation temperature and pressure, through a system of tubes filled with different pressures. Shockwaves formed by these tubes can achieve very high Mach numbers.

In general, the high temperature created by the shockwave allows the dissociation of molecules of N_2 and O_2 present in the air, however, the temperature is not enough to do a direct ionization. Under these circumstances, it is used an ion sensor to create a voltage potential between two electrodes and thus permitting the ionization of the air.

Most of the studies concerning ion sensors are related to shockwave speed measurement without consideration of the details of the flow conditions which they are imparted. In this paper, we show the development of an ionization sensor for shock tube applications. The tests were done in the shock tube T1 with the main objective of observing the response of the sensor under stagnation conditions, thus obtaining its voltage response in high temperatures.

3. METHODOLOGY

3.1 Ionization sensor

The ionization sensor is shown in Fig. 1. The sensor is comprised of two electrodes of tungsten-thorium (Ø1 mm), mounted diametrically opposite, and 1.0 mm apart. This material was chosen due to its capability to support high temperatures with low erosion. In addition to that, the thorium helps the passage of electric current and also gives more stability and longevity to the sensor. This kind of electrode is widely used in TIG welding. Also, it was used an alumina ceramic material for a good electrical and thermal insulation even at high temperatures. The electrodes were fixed to the ceramic with a bicomponent epoxy resin. Two seal-rings were used for sealing the sensor. Moreover, it was fabricated with stainless steel clamp nut for adequate seal and an adapter for the sensor to be used in the shock tube.

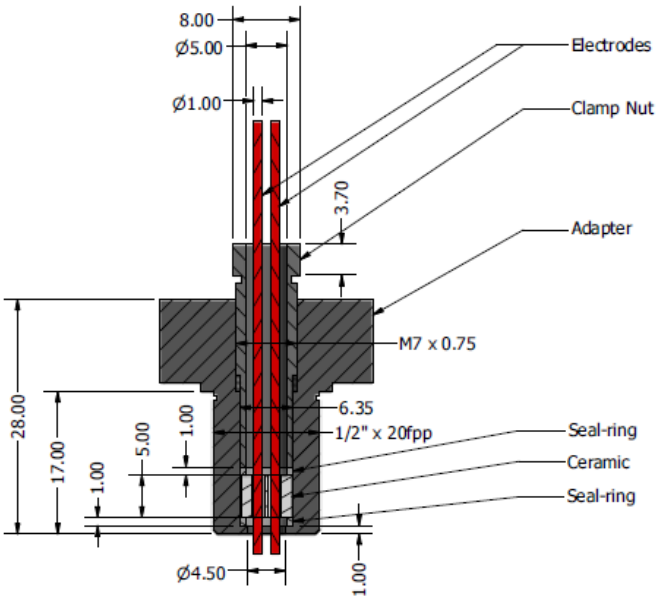

Figure 1: Sectional view of the produced ionization sensor. Dimensions in mm.

The Fig. 2 shows the electrical circuit used for the tests. The choice of the voltage, resistances and capacitor was based on the work of Glass and Hall (1959). These values provide quick response of the sensor, high voltage between the electrodes and a high level output signal. In this circuit, the discharge time can be estimated using the Eq. (1), and the charge time can be estimated using the Eq. (2), below:

$$\tau_{discharge} = (47\times10^{3}\Omega)(0.5\times10^{-9}\,\mathrm{F}) = 23.5\mu s \quad (1)$$

$$\tau_{charge} = (10\times10^{6}\,\Omega)(0.5\times10^{-9}\,\mathrm{F}) = 5\,ms \quad (2)$$

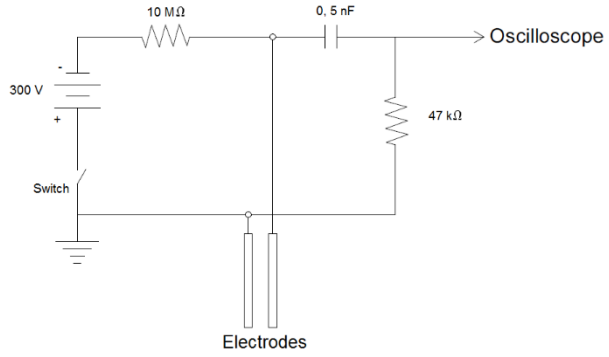

Figure 2: Electrical circuit used with the ionization sensor.

The electrical circuit presents high level of noise when the switch is on, to circumvent that the switch was turned off after the capacitor charging, during the tests. Since the circuit is in open loop, the capacitor will not discharge until ionization of the air.

3.2 Shock tube description

During these tests we used the shock tube T1, see Fig. 3. This tube is comprised of two reservoirs, one at a high pressure denominated driver and the other one with a lower pressure denominated driven. These two reservoirs are separated by a DDS (Double Diaphragm Section), in which two diaphragms with known rupture pressures are used to control the test start. This section remains at an intermediate pressure. The entire tube has an internal diameter of 68.00 mm. The driver section has a length of 2219.10 mm, the driven section has length of 2853.45 mm and the DDS has 35.70 mm.

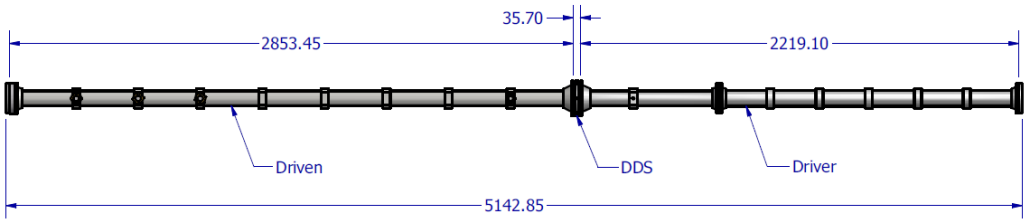

Figure 3: Dimensions of shock tube T1, in mm.

After the diaphragm rupture, a shockwave is formed and moves from the DDS to the driven and modifies the properties of the initial gas, denominated region 1, the thermodynamic properties of the disturbed gas, denominated region 2, as shown in Fig. 4(a), can be calculated based on the initial properties and the velocity of the incident shockwave measured experimentally. When the incident shockwave reaches the end of the shock tube driven, it reflects and modifies the properties of the flow in region 2, moreover, it creates a new region denominated region 5, as shown in Fig. 4(b), which has the test conditions for the ionization sensor.

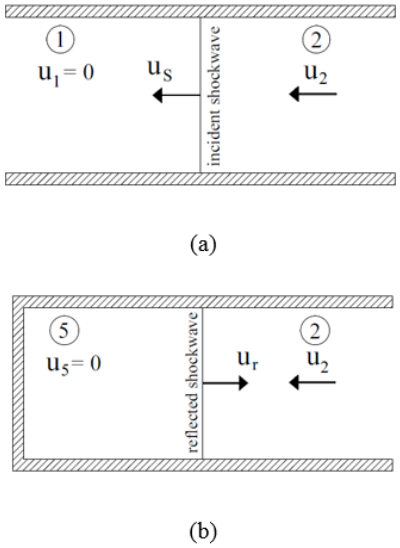

Figure 4: Shockwave system inside shock tube: (a) Incident shockwave and (b) Reflected shockwave.

The properties across the incident and reflected shockwaves (regions 2 and 5, respectively) are calculated considering chemical equilibrium. The air is modeled as a mixture of gases, N_2, O_2, NO, N, O and Ar, and the final composition is calculated through Gibbs free energy minimization, details about this procedure are given in Rolim (2013). The thermodynamic properties of each species were calculated with the NASA polynomials described by Gordon and McBride (1993) with updated coefficients given by the thermochemical database of Burcat and Ruscic (2005).

3.3 Experimental apparatus

The experimental apparatus for the tests is presented in Fig. 5 with the ionization sensor positioned in the end of the driven. It was used three piezoelectric sensors type PCB 113B26 (PCB PIEZOTRONICS, 2013) to measure the pressure along the tube and to estimate the velocity of incident shockwave by time of flight (TOF). The choice of a piezoelectric sensor was due to its fast response required in studies of shockwaves. The data acquisition system was a Yokogawa oscilloscope type DL750 ScopeCorder with 16 channels, using a signal conditioner type PCB 481 for the pressure sensors. Also, it was used an ultrastable power supply type 70706 to provide 300 V to the circuit. On later tests this power supply was substituted by a power supply fabricated in-house, which has a ripple factor of 1%.

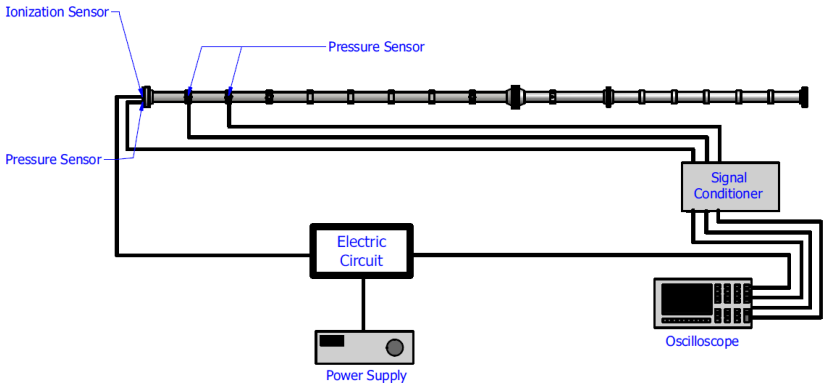

Figure 5: Schematics of the shock tube tests.

The positions of the pressure sensors along the tunnel are shown in Fig. 6, where P5 is in the end of the driven and the others sensors are positioned along the driven, P2.2 closer to the end, P2.1 in the middle and P2.0 in a further position. However, only the pressure signal from the position P2.2 was used for incident shockwave pressure measurement and the pressure signal from the position P5 was used for reflected shockwave pressure measurement. In the Tab. 1, it is shown the technical specifications of the pressure sensors used during the tests.

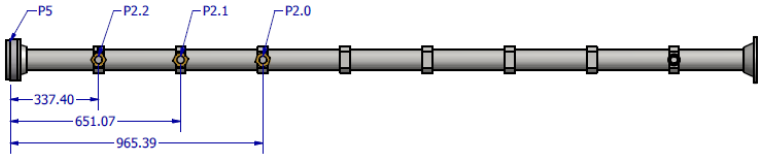

Figure 6: Position of the pressure sensors along the driven. Dimension in mm.

Table 1: General specification of the sensor PCB113B26 (PCB PIEZOTRONICS, 2013)

Measurement range	500 psi
Sensitivity	10 mV/psi
Maximum Pressure	10,000 psi
Resolution	2 mpsi
Discharge Time Constant	≥50 s
Rise Time	≤1μs
Output Impedance	< 100 Ω
Uncertainty	±1.3%

It was possible to determine the incident shockwave velocity u_s by measuring the time interval between the signals from the first sensor and from the second sensor Δt, since the distance between them was known, equal to Δx, one can get the incident shockwave velocity using Eq. (3):

$$u_s = \frac{\Delta x}{\Delta t} \tag{3}$$

3.4 Test matrix

Table 2 shows that the only parameter varied during this investigation was the initial driven pressure. The choice of positioning the sensor at the end of the driven section is justified because the reflected shockwave produces a higher temperature than the incident shockwave, which helps ionization (Anderson, 1989).

Table 2: Test conditions

Number of valid tests	Initial pressure in driven [kgf/cm²]	Gas in driven	Initial pressure in driver [kgf/cm²]	Gas in driver	Condition
12	1.0	Synthetic air	70	Helium	Reflected shockwave
4	1.2	Synthetic air	70	Helium	Reflected shockwave
5	1.5	Synthetic air	70	Helium	Reflected shockwave

4. DISCUSSION OF RESULTS

For these tests, the driven was filled with synthetic air at the pressures of 1.0, 1.2 and 1.5 kgf/cm². The driver was filled with helium at the pressure of 70 kgf/cm². The shock tube conditions achieved during these tests are shown in Tab. 3, where one can see the initial conditions, the conditions after incident shockwave and the conditions after reflected shockwave. Uncertainties were calculated using the methodology presented by AIAA S-071A-1999 (AIAA, 1999), working with a confidence level at 95%.

Table 3: Estimated properties calculated for initial driven pressures of 1.0, 1.2 and 1.5 kgf/cm²

Parameter	Test condition with 1.0 kgf/cm²	Test condition with 1.2 kgf/cm²	Test condition with 1.5 kgf/cm²	Unit
p_1	$9.81 \times 10^4 \pm 9.81 \times 10^3$	$1.18 \times 10^5 \pm 9.81 \times 10^3$	$1.47 \times 10^5 \pm 9.81 \times 10^3$	Pa
T_1	293.92 ± 0.81	299.65 ± 2.26	299.55 ± 2.06	K
ρ_1	1.16 ± 0.12	1.37 ± 0.11	1.71 ± 0.11	kg/m³
u_s	970.21 ± 33.60	995.63 ± 30.96	942.05 ± 35.15	m/s
M_s	2.82 ± 0.10	2.87 ± 0.09	2.71 ± 0.10	-
a_1	343.76 ± 0.47	347.08 ± 1.33	347.02 ± 1.19	m/s
Air properties after incident shockwave				
p_2	$1.07 \times 10^6 \pm 7.56 \times 10^4$	$1.20 \times 10^6 \pm 1.75 \times 10^4$	$1.34 \times 10^6 \pm 4.35 \times 10^4$	Pa
T_2	853.27 ± 107.41	795.93 ± 70.97	748.02 ± 61.09	K
ρ_2	4.38 ± 0.46	5.23 ± 0.46	6.24 ± 0.47	kg/m³
u_2	712.80 ± 32.27	735.43 ± 29.70	683.85 ± 34.02	m/s
h_2	$5.82 \times 10^5 \pm 1.19 \times 10^5$	$5.18 \times 10^5 \pm 7.79 \times 10^4$	$4.66 \times 10^5 \pm 6.63 \times 10^4$	J/kg
Air composition after incident shockwave				
N_2	$1.18 \times 10^2 \pm 1.23 \times 10^1$	$1.41 \times 10^2 \pm 1.24 \times 10^1$	$1.68 \times 10^2 \pm 1.26 \times 10^1$	mol/m³
O_2	$3.18 \times 10^1 \pm 3.31$	$3.80 \times 10^1 \pm 3.34$	$4.53 \times 10^1 \pm 3.39$	mol/m³
O	$1.89 \times 10^{-11} \pm 8.24 \times 10^{-11}$	$1.66 \times 10^{-12} \pm 5.47 \times 10^{-12}$	$1.63 \times 10^{-13} \pm 5.27 \times 10^{-13}$	mol/m³
Ar	$1.51 \pm 1.58 \times 10^{-1}$	$1.81 \pm 1.59 \times 10^{-1}$	$2.16 \pm 1.62 \times 10^{-1}$	mol/m³
NO	$7.14 \times 10^{-4} \pm 1.10 \times 10^{-3}$	$3.38 \times 10^{-4} \pm 3.86 \times 10^{-4}$	$1.66 \times 10^{-4} \pm 1.88 \times 10^{-4}$	mol/m³
N	$6.43 \times 10^{-25} \pm 5.36 \times 10^{-24}$	$5.81 \times 10^{-27} \pm 3.67 \times 10^{-26}$	$6.56 \times 10^{-29} \pm 4.05 \times 10^{-28}$	mol/m³
Air properties after reflected shockwave				
p_5	$4.65 \times 10^6 \pm 4.06 \times 10^5$	$5.35 \times 10^6 \pm 1.19 \times 10^5$	$5.73 \times 10^6 \pm 1.27 \times 10^5$	Pa
T_5	1347.51 ± 235.92	1239.22 ± 160.96	1151.39 ± 139.82	K
ρ_5	12.0 ± 1.8	15.0 ± 1.9	17.3 ± 2.1	kg/m³
u_r	408.33 ± 26.36	392.85 ± 17.71	385.03 ± 16.63	m/s
h_5	$1.15 \times 10^6 \pm 2.83 \times 10^5$	$1.03 \times 10^6 \pm 1.90 \times 10^5$	$9.22 \times 10^5 \pm 1.63 \times 10^5$	J/kg
Air composition after reflected shockwave				
N_2	$3.24 \times 10^2 \pm 4.93 \times 10^1$	$4.05 \times 10^2 \pm 5.19 \times 10^1$	$4.67 \times 10^2 \pm 5.58 \times 10^1$	mol/m³
O_2	$8.71 \times 10^1 \pm 1.34 \times 10^1$	$1.09 \times 10^2 \pm 1.40 \times 10^1$	$1.26 \times 10^2 \pm 1.50 \times 10^1$	mol/m³
O	$1.13 \times 10^{-5} \pm 4.30 \times 10^{-5}$	$1.82 \times 10^{-6} \pm 5.59 \times 10^{-6}$	$3.12 \times 10^{-7} \pm 9.64 \times 10^{-7}$	mol/m³
Ar	$4.15 \pm 6.30 \times 10^{-1}$	$5.19 \pm 6.64 \times 10^{-1}$	$5.98 \pm 7.14 \times 10^{-1}$	mol/m³
NO	$2.21 \times 10^{-1} \pm 2.87 \times 10^{-1}$	$1.36 \times 10^{-1} \pm 1.39 \times 10^{-1}$	$7.94 \times 10^{-2} \pm 8.28 \times 10^{-2}$	mol/m³
N	$4.55 \times 10^{-14} \pm 3.33 \times 10^{-13}$	$1.28 \times 10^{-15} \pm 7.54 \times 10^{-15}$	$4.17 \times 10^{-17} \pm 2.47 \times 10^{-16}$	mol/m³
Ionization sensor				
Voltage	$1.81 \times 10^{-2} \pm 8.99 \times 10^{-3}$	$1.97 \times 10^{-2} \pm 1.31 \times 10^{-2}$	$8.29 \times 10^{-3} \pm 2.75 \times 10^{-3}$	V

Comparing the Mach number values of experiments with initial driven pressures of 1.0 kgf/cm² and 1.2 kgf/cm², it was observed that the average Mach number of 1.2 kgf/cm² was 2.87, while the average Mach number of 1.0 kgf/cm² was

2.82. However, it was expected that the Mach number value at 1.0 kgf/cm² would be higher than that obtained for 1.2 kgf/cm², the authors believe that the variation of the initial driven temperature (T_1) contributed to this result.

In Fig. 7, a response of the ionization sensor for the test condition of initial driven pressure of 1.0 kgf/cm² is shown. The passage of incident and reflected shockwave from the piezoelectric sensors signal was observed. Also, it can be noted that the response of ionization sensor under stagnation conditions imposed by the shock is matching with response of piezoelectric sensors.

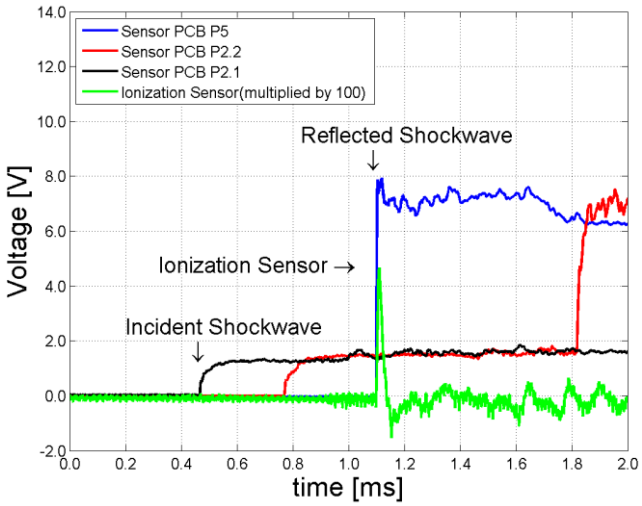

Figure 7: Voltage history for the ionization and pressure sensors with initial driven pressure of 1.0 kgf/cm².

With the average values presented at Tab. 3, the sensor signal was analyzed with the variation of the initial driven pressures, temperature and air density in stagnation condition, the results are shown in Fig. 8, Fig. 9 and Fig. 10, respectively.

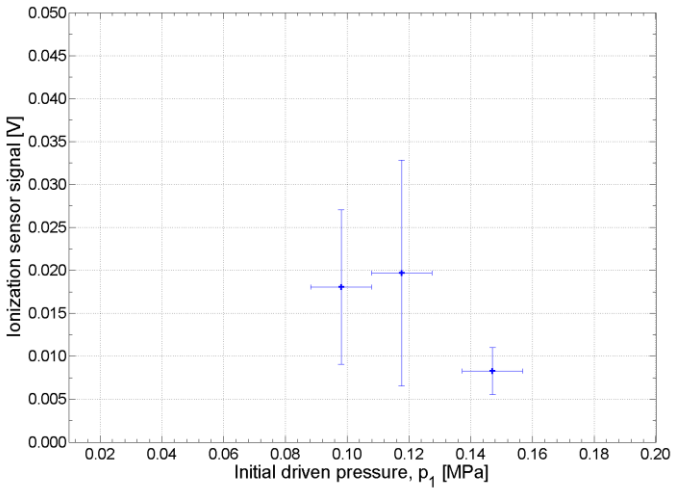

Figure 8: Variation of ionization sensor signal with the initial driven pressure.

In Fig. 8, it is possible to observe that the signal decreases from 1.81×10^{-2} to 8.29×10^{-3} V (54.2%) when varying the initial driven pressure from 1.0 kgf/cm² (9.81×10^{-2} MPa) to 1.5 kgf/cm² (1.47×10^{-1} MPa) probably due to the decrease of stagnation temperature. However, for the cases of the initial driven pressure varied from 1.0 kgf/cm² (9.81×10^{-2} MPa) to 1.2 kgf/cm² (1.18×10^{-1} MPa) the signal increases from 1.81×10^{-2} to 1.97×10^{-2} V (8.8%).

It was expected that the ionization sensor when exposed to higher temperatures would present higher voltage amplitudes, because the high temperature helps the ionization of the air (Anderson, 1989). In Fig. 9, it is shown the variation of sensor signal with the stagnation temperature obtained during the tests. It is observed that the signal increases from 8.29×10^{-3} to 1.97×10^{-2} V (137.6%) with the elevation of temperature from 1151.39 to 1239.22 K, however, it decreases from 1.97×10^{-2} to 1.81×10^{-2} V (8.1%) from 1238.22 to 1347.51 K. Similarly, in higher air densities, it was expected that sensor would present higher voltage amplitudes due to the increase of the total molar concentration, see Tab. 3 for air composition after reflected shockwave, note that the molar concentrations of N_2, O_2 and Ar are much higher than those from other species. In Fig. 10, it is shown the variation of the sensor signal with the stagnation air density, where an increase of the signal is observed when the air density varies from 12.0 to 15.0 kg/m³, on the other hand, the

signal decreases when density varies from 15.0 kg/m³ to 17.3 kg/m³. Observing Fig. 9 and Fig 10 one can see a relation type "mirror" between the graphs of temperature and density, this happens because of the fact that in this kind of shock tube operation the temperature decrease when the air density rises, as can be seen in Fig. 11. Thus, for higher temperatures, there is a drop in air density, which reduces the voltage amplitude and justifies that the point with initial driven pressure of 1.2 kgf/cm² presented the highest voltage amplitude.

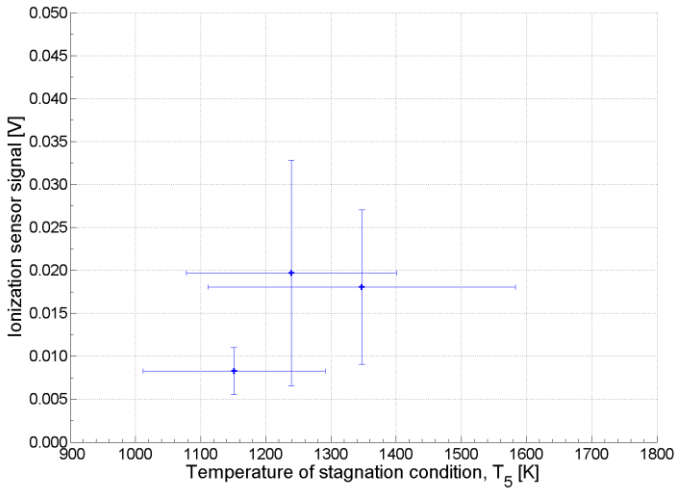

Figure 9: Variation of the ionization sensor signal with stagnation temperature.

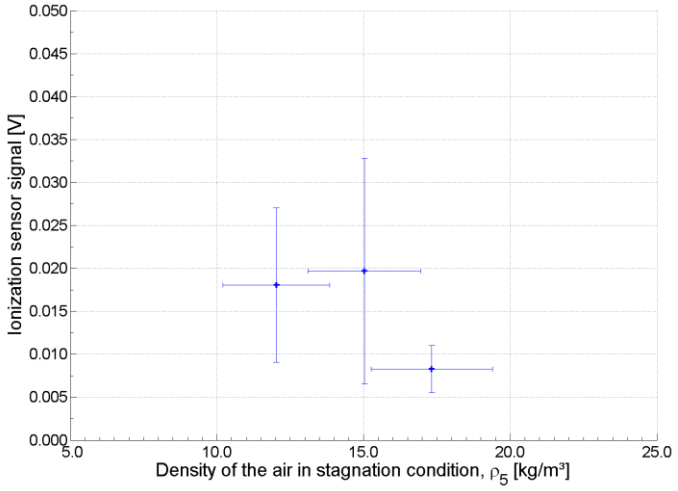

Figure 10: Variation of the ionization sensor signal with stagnation air density.

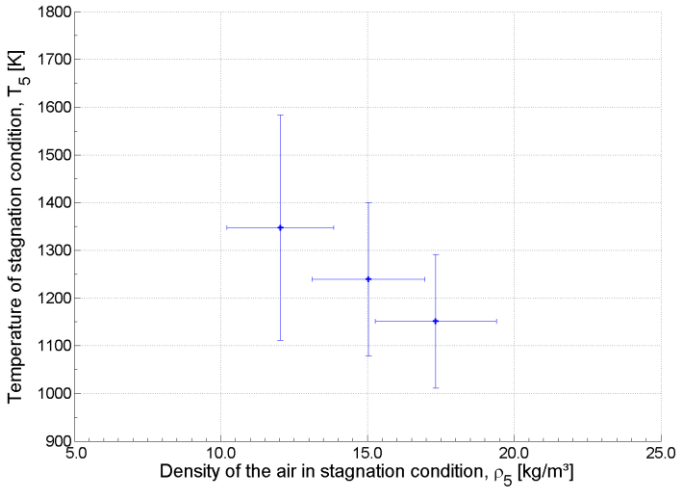

Figure 11: Relationship between the stagnation temperature and the stagnation air density.

5. CONCLUSIONS

Using the ionization sensor developed in this work, in a shock tube under stagnation conditions, it was possible to observe the behavior of the sensor when exposed to air at high temperatures. The stagnation temperatures varied from 1151.39 to 1347.51 K and the stagnation pressures from 4.65 to 5.73 MPa. Also, it was possible to conclude that the response of the ionization sensor signal was fast and consistent.

In principle, it was expected that the signal from the sensor would be higher when exposed to higher temperatures. However, the air density influenced the sensor signal; in this work, the air density and temperature varied inversely under stagnation conditions, and lower densities would produce less ions in the air. Therefore, when the temperature was increased, the air density decreased, the results of the sensor were a balance between these two effects.

For future experiments, this ionization sensor will be used to capture the signal of the incident shockwave, to measure the speed of the shockwave.

6. ACKNOWLEDGEMENTS

The authors would like to express their gratitude to GIA-SJ for your founding support. Also, thanks to Carla S. T. Marques, Sgt. Joely E. Ferraz, Marcos V. R. Santos, Luiz C. M. Lavras, Valéria S. F. O. Leite, José B. Chanes Jr and Jaime T. Watanuki for their contribution along this project.

7. REFERENCES

AIAA, 1999. Assessment of Experimental Uncertainty With Application to Wind Tunnel Testing. AIAA Standard S-071A-1999. Reston.

Anderson, J.D., 1989 Hypersonic and High Temperature Gas Dynamics. McGraw-Hill 2nd ed. London. UK.

Burcat, A. and Ruscic, B., 2005. Third Millennium Ideal Gas And Condensed Phase Thermochemical Database For Combustion With Updates From Active Thermochemical Tables. ANL-05/20 and TAE 960. Argonne: Argonne National Laboratory and Technion-IIT. Report.

Glass, I. I. and Hall, J. G., 1959. Handbook of Supersonic Aerodynamics. Johns Hopkins University Applied Physics Laboratory.

Gupta, N. K. M., 2013. Point Measurement of Detonation Wave Propagation Using Ion Gauge. Master dissertation, The University of Texas At Arlington, Arlington, USA.

McBride, B.J., Gordon S. and Reno, M.A., 1993. Coefficients For Calculating Thermodynamic And Transport Properties of Individual Species. NASA-TM-4513. Cleveland: NASA.

Panicker, P. K., 2008. The Development and Testing of Pulsed Detonation Engine Ground Demonstrators. Ph.D. thesis, The University of Texas At Arlington, Arlington, USA.

PCB PIEZOTRONICS, 2013. Model 113A26 ICP Pressure Sensor Installation and Operating Manual.

Rolim, T.C., 2013. Investigation Of Side Wall Effects On An Inward Scramjet Inlet At Mach Number 8.6, 232f. Doctoral Dissertation. The University of Texas at Arlington, Arlington, USA.

8. RESPONSIBILITY NOTICE

The authors are the only responsible for the printed material included in this paper.